



A Unified Mechanism for Spontaneous-Rate and First-Spike Timing in the Auditory Nerve

B. SURESH KRISHNA

Center for Neural Science, New York University, New York, NY 10003, USA

suresh@cns.nyu.edu

Received September 27, 2001; Revised April 4, 2002; Accepted May 10, 2002

Action Editor: Shihab Shamma

Abstract. Recent physiological experiments have provided detailed descriptions of the properties of first-spike latency and variability in auditory cortex and nerve in response to pure tones with different envelopes. The envelope-dependence of first-spike timing and precision in auditory cortical neurons appears to reflect properties established in the nerve. First-spike latency properties in individual auditory nerve fibers are strongly correlated with their spontaneous rate (SR). It is shown here that a minimal, plausible model of auditory transduction with two free parameters accurately reproduces the physiological data from the auditory nerve population. The model consists of a simple gain stage, a bandpass filter, a rectifying saturating non-linearity, and a lowpass filter in series. The output of the lowpass filter drives an inhomogeneous Poisson process. The shape of the non-linearity is determined by SR; in physiological terms, this shape depends upon the resting sensitivity of the synapse between the inner hair cell and the auditory nerve. An alternative model for SR generation, where SR is added to the stimulus-driven output of a fixed nonlinearity, fails to account for the data. The results provide a novel, comprehensive and physiologically-based explanation for the range of experimental results on the envelope-dependence of first-spike latency and precision, and its relationship with SR, in the auditory system.

Keywords: spike timing, auditory nerve, spontaneous-rate, auditory cortex, latency

Introduction

First-spike latency (henceforth referred to simply as “latency”) has been explored as a neural code in many sensory systems (e.g. audition: Brugge et al., 1996; Eggermont, 1998a; Furukawa et al., 2000; vision: Gawne et al., 1996; Reich et al., 2001; olfaction: Hopfield, 1995; somatosensation: Panzeri et al., 2001). Bilateral latency differences are implicated in sound localization (Joris et al., 1998; Mason et al., 2001) and the Pulfrich effect (Anzai et al., 2001). Transient spike-timing assumes special importance in audition because ecological warning sounds are often brief; thus transient, rapidly-transmitted, and precisely-timed spike responses may be essential for warning detection and localization.

In general, latency decreases as stimulus intensity increases (e.g. audition: Heil and Irvine, 1997; Klug et al., 2000; vision: Maunsell et al., 1999; Warzecha and Egelhaaf, 2000; somatosensation: Mountcastle et al., 1957). In audition, the relationship between latency and sound pressure level (SPL) for pure tones has been studied in detail in many brain regions (e.g. Heil and Irvine, 1996; Klug et al., 2000). Since latency decreases with intensity, intensity differences between the two ears also create latency differences between the two ears. This has led to the suggestion that binaural intensity differences can be detected by a comparator mechanism that detects timing differences between the two ears. In principle, this comparator could be similar or identical to the interaural timing comparator that underlies azimuthal sound localization of low-frequency tones.

Using this idea of “time-intensity trading”, functions relating latency to stimulus intensity have been derived from psychophysical studies (e.g. David et al., 1959).

If latency forms a coding mechanism, the standard-deviation of latency (henceforth simply “standard-deviation”: Bair, 1999; Heil and Irvine, 1997; Phillips and Hall, 1990) is a measure of noise in the latency code. Standard-deviation increases systematically with latency in many auditory areas (e.g. Heil and Irvine, 1997, 1998; Phillips and Hall, 1990).

Latency and standard-deviation also depend on rise-time (auditory cortex: Heil, 1997a; nerve: Heil and Irvine, 1997; cochlear nucleus: Kitzes et al., 1978), i.e. time for sound to reach maximum SPL from onset. For tones varying in SPL and rise-time, latency and standard-deviation in cortex are functions of a single variable: maximum velocity of peak pressure (MVPP) for linear rise-envelopes or maximum acceleration of peak pressure (MAPP) for cosine-squared rise-envelopes (Heil, 1997a). The dependence upon MAPP for cosine-squared rise-envelopes has also been found in the auditory nerve (Heil and Irvine, 1997). Because of many similarities in response properties between auditory nerve and cortex, it has been suggested that cortical responses may simply reflect dependencies generated in the nerve (Heil and Irvine, 1997). The functions relating latency (and standard-deviation) to maximum acceleration for individual auditory nerve fibers show strong correlations with their SR.

Auditory nerve fibers show a markedly bimodal distribution of SRs (Lieberman, 1978). Various correlations of response properties with SR have been observed; for example, high-SR fibers show lower thresholds and steeper increases in firing rate with sound intensity. These variations in firing properties lead to variations in their ability to encode sound properties, and are considered to be important for the maintenance of auditory function over a wide range of SPLs (Cooper et al., 1993; Sachs, 1984; Sachs et al., 1989; Yates, 1991). It is known that fibers with varying SRs can synapse onto a single hair cell; thus differences in SR probably arise from differences in the properties of the synapse between the hair cell and the nerve fiber. Such differences have been identified; synapses from fibers with different SRs can be distinguished on the basis of their size, morphology, and location on the inner hair cell (Lieberman, 1982; Lieberman et al., 1990; Merchan-Perez and Lieberman, 1996).

This paper proposes a minimal computational mechanism that accounts quantitatively for first-spike tim-

ing and precision, and its relationship with SR, in the auditory nerve. In the model, both SR and the properties of first-spike latency depend critically on a single parameter that controls the shape of a static nonlinearity in the auditory periphery. Physiologically, the variation in shape reflects differences in the gain properties of the synapse between the inner hair cell and the auditory nerve; this shape is determined by SR. An alternative model where SR is added to the stimulus-driven output of a fixed nonlinearity fails to account for the experimental data. The modeling results provide a comprehensive physiologically-based explanation for almost all the existing data on first-spike timing and its relationship to SR. Further, the results clarify a variety of issues raised by the physiological data. The model also provides a structural basis that is consistent with experimental data, for the establishment of a “latency code” for stimulus intensity (and rise-time).

Methods

Model Structure: Overview

The model consists of four stages connected together in series: a simple gain stage that changes the SPL of the input stimulus, a bandpass filter, a rectifying, saturating static nonlinearity, and a lowpass filter (Fig. 1). The output of the lowpass filter is used as the rate-function for an inhomogeneous Poisson process to generate the first-spike. This general form has also been used in other physiological (e.g. Shamma et al., 1986) and psychophysical (e.g. Oxenham and Plack, 2000) models. The gain stage represents the effects of external/middle-ear filtering (Rosowski, 1991); the magnitude of gain depends upon characteristic frequency (CF). The bandpass filter mimics basilar membrane filtering. The nonlinearity represents the concatenation of three different fast-acting nonlinear stages in the auditory periphery: basilar membrane compression (Rhode and Recio, 2000), the inner hair cell’s rectifying, compressive, current-voltage relationship (e.g. Dallos and Cheatham, 1989) and synaptic rectification (spike-rates cannot be negative). Finally, the lowpass filter represents the lowpass filtering effects of the inner hair cell membrane and the auditory nerve synapse.

Gain Stage and Bandpass Filter

The first stage of the model acts as a simple gain stage. The examples of model and experimental data

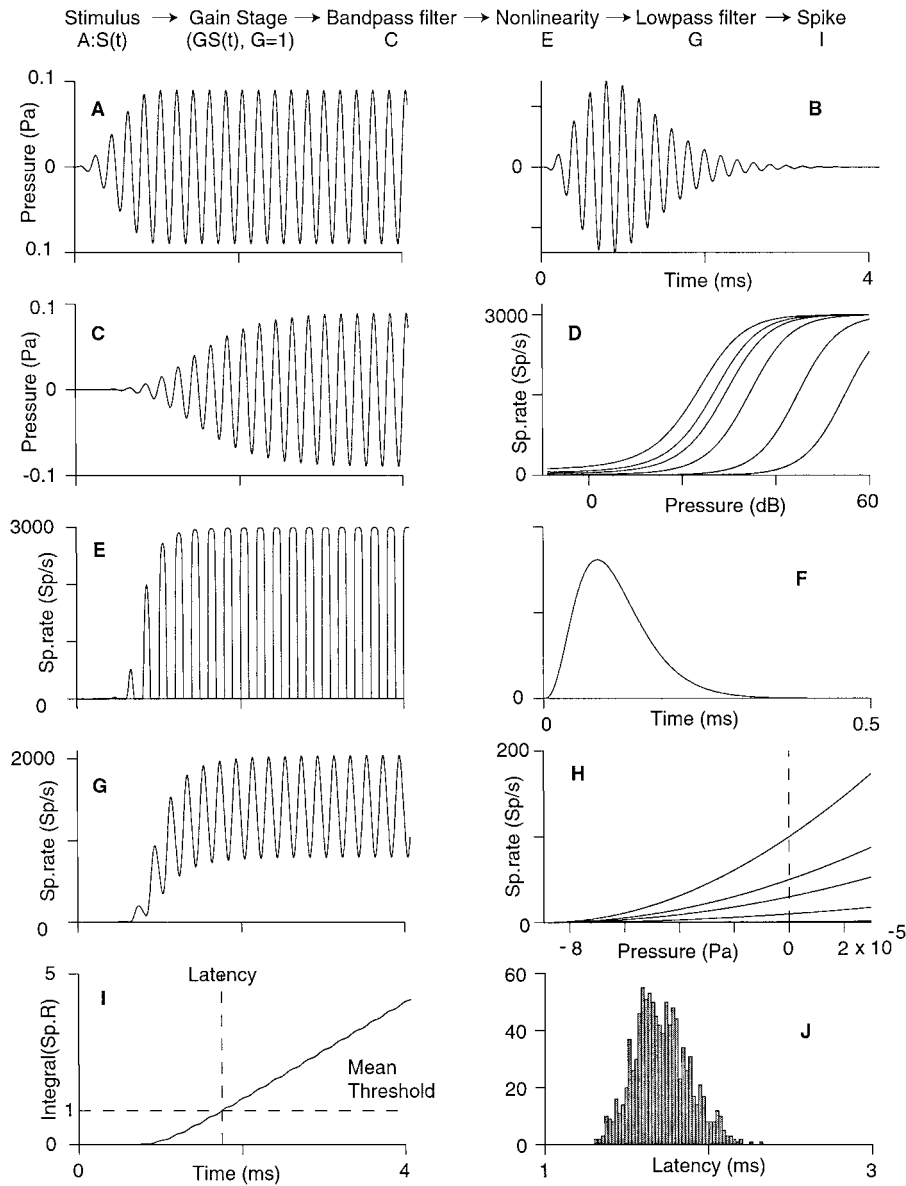


Figure 1. The model and its responses. Model structure shown in flowchart form on top; gain stage omitted from figures because its gain G is set to 1 (see Methods). **A:** Example stimulus: 30 dB, 5 kHz tone, cosine-squared rise-envelope (1 ms rise-time). **C, E, G** and **I:** Model output after bandpass filtering, nonlinear rectification, lowpass filtering, and integration to the exponentially distributed spike-threshold respectively. **B:** 5 kHz CF gammatone filter's impulse response. **D:** Michaelis-Menten nonlinearity's input-output function at 6 SRs (left to right: .1, 1, 10, 30, 50, 100 spikes/second). **F:** Lowpass filter impulse response (4th order, corner frequency = 2500 Hz). **H:** D magnified around 0 Pa; SR is nonlinearity's output at 0 stimulus-pressure. **J:** Model latency distribution (from 1000 repetitions). **A, C, E, G** and **I** have identical abscissas; see **I** for axis label. **I:** Y axis is the integral of spike-rate with respect to time. Throughout, Sp/s = spikes/second and Sp.rate = Spike-rate.

shown in this paper (Figs. 2 and 3) come from auditory nerve-fibers with characteristic frequency (CF) around 8 kHz; the magnitude G of the gain is set to be 1 for these data (i.e. the stimulus passes through the gain stage unchanged). The value of the gain G at other frequencies is estimated from the data (Fig. 5); the

dependence of G on CF is roughly similar to published psychophysical and N1 audiograms for the cat (see Discussion).

The bandpass filter is modeled as a gammatone filter centered at CF (Patterson et al., 1988: as implemented in Malcolm Slaney's Auditory Toolbox for MATLAB).

The gammatone filter is characterized by its impulse response $g(t)$ (Fig. 1B):

$$g(t) = t^3 \cos(\omega t) e^{-bt} \quad (1)$$

$$\omega = 2\pi(CF), \quad b = 1.019(2\pi)((CF/Q) + W)$$

t is time (here and *throughout this paper*). Q was set to 9.2645, and W to 24.7 (Glasberg and Moore, 1990). This filter has maximum gain at CF. The parameter b in the gammatone impulse response increases with CF; therefore, the width of the impulse response decreases with CF. Over most of the range of frequencies considered in this paper, the impulse response is narrow (e.g. Fig. 1B), and therefore the effect of this filter on latency and standard-deviation are small (a few milliseconds, at most. Fig. 1C). Reasonable variations of filter parameters produce negligible changes in the results. Note that since the width of the impulse response decreases with CF, the bandwidth increases with CF.

Static Nonlinearity

The static nonlinearity is modeled as a Michaelis-Menten function. The input-output function (i.e. function that gives the output $y(t)$ of the nonlinearity for a given input $x(t)$) of this nonlinearity is (Fig. 1D and H):

$$y(t) = R_{\max}(x(t) - x_0)^2 / ((x(t) - x_0)^2 + K_m), \quad x(t) \geq x_0 \quad (2)$$

$$y(t) = 0, \quad x(t) < x_0$$

R_{\max} = Maximum firing rate (spikes/second), Input $x(t)$ = Output of gammatone filter R_{\max} was set to 3000 spikes/second (see: Gaumont et al., 1983 for plausibility of this value); values much lower than this produced inordinately high minimum latency and standard-deviation (Fig. 8). Setting x_0 to a value of around -89.44μ Pa (which is the minimum pressure attained by a 10 dB tone) gave a good fit to 2 example fibers (Figs. 2 and 3 in Heil and Irvine, 1997: Figs. 2 and 3 here). As shown below, varying x_0 is identical to varying G (the gain of the first gain stage). Therefore, x_0 is fixed at this value for the rest of the paper; all manipulations of this parameter are achieved by varying the value of G . K_m is determined by SR and x_0 (see below). Since x_0 is fixed, SR determines the shape of the nonlinearity.

Lowpass Filter and Spike-Generation

The lowpass filter is a fourth-order polynomial filter with a corner frequency of 2500 Hz and is derived from data on synchronization to pure tones in the cat (Weiss and Rose, 1988). It is defined by its impulse response $l(t)$ (Fig. 1F):

$$l(t) = (1/\tau)^4 (t^3/6) (e^{-t/\tau}), \quad \tau = 0.027 \text{ ms} \quad (3)$$

The output of the lowpass filter (Fig. 1G) is used as the rate-function for an inhomogeneous Poisson process. This is implemented by integrating the filter output until it crosses a threshold value that is drawn from an exponential distribution with mean 1 (Johnson, 1996). This threshold-crossing time gives latency (Fig. 1I). Since the threshold is random, the threshold-crossing times are also random; thus latency varies from one stimulus-presentation to the next (Fig. 1J). The mean and standard-deviation of latency are estimated, for a given stimulus, from many stimulus repetitions.

Since only the first spike is modeled, spike-history effects (including refractory period) are ignored so as to minimize the number of parameters. Spike-history effects are only relevant to the extent that the response spike (first spike following stimulus onset) may occur shortly after a spontaneous spike that immediately preceded stimulus presentation. However, even at high SRs, this has a very low probability of occurring. Spike-history effects are therefore assumed to be negligible.

SR Fully Determines the Shape of the Nonlinearity

Notice the model SR is simply the steady output of the lowpass filter when there is no stimulus. The lowpass filter's gain to steady input is 1. Therefore when there is no stimulus, the output of the lowpass filter is identical to its steady input, which in turn is the steady output of the static nonlinearity. The output $y(t)$ of the static nonlinearity when its input $x(t)$ is zero, i.e. when there is no stimulus, is given by:

$$y(t) = SR = R_{\max}(x_0^2 / (x_0^2 + K_m)) \quad (4)$$

$$\text{Rearranging: } K_m = x_0^2 (R_{\max}/SR - 1) \quad (5)$$

Thus, since x_0 is fixed, once SR is known (i.e. estimated from experimental data, for an individual auditory nerve fiber), K_m is completely determined. The resulting dynamic ranges of the nonlinearity at different SRs (Fig. 1D) are not inconsistent with the dynamic ranges seen in existing experimental

descriptions of onset responses in the auditory nerve (Smith and Brachman, 1980). Incidentally, fixing K_m and letting x_0 vary with SR produced poor fits to the population data (not shown).

Varying x_0 is Identical to Varying G

If the stimulus is scaled by G , then the output of the gammatone filter is also scaled by G , because it is a linear filter. The output of the gammatone filter forms the input $x(t)$ for the static nonlinearity. Thus:

If $x(t)$ is scaled to $Gx(t)$, where G is a gain factor, then

$$y(t) = R_{\max}(Gx(t) - x_0)^2 / ((Gx(t) - x_0)^2 + K_m), \quad Gx(t) \geq x_0 \quad (6)$$

$$y(t) = 0, \quad Gx(t) < x_0$$

Rearranging,

$$y(t) = R_{\max}(x(t) - x_0/G)^2 / ((x(t) - x_0/G)^2 + K_m/G^2), \quad x(t) \geq x_0/G \quad (7)$$

$$y(t) = 0, \quad x(t) < x_0/G$$

Recall from (5) that $K_m = x_0^2(R_{\max}/SR - 1)$, so setting $x_0/G = x'_0$,

$$y(t) = R_{\max}(x(t) - x'_0)^2 / ((x(t) - x'_0)^2 + K'_m), \quad K'_m = x_0^2(R_{\max}/SR - 1), \quad x(t) \geq x'_0 \quad (8)$$

$$y(t) = 0, \quad x(t) < x'_0$$

Scaling x_0 by $1/G$ is thus identical to multiplying stimulus amplitude by G .

Alternative Model

An alternative model is also examined (and rejected on the basis of the experimental data). In this model, the stimulus-driven stages are all fixed. In particular, the parameters of the static nonlinearity are not regulated by SR; SR is instead added to the output of the nonlinearity. The nonlinearity is shown in Fig. 6A. x_0 is set to $-15.9 \mu\text{ Pa}$ (minimum peak pressure of a -5 dB tone) and K_m (now a fixed parameter) to $7.59 \times 10^{-6} \text{ Pa}^2$. This set of values provides a good fit to the experimental responses in Fig. 2. Since the spontaneous output of the nonlinearity with this set of parameters is 0.1 spikes/second, 0.1 is subtracted from the output of the nonlinearity to ensure zero spontaneous output.

Thus, the nonlinearity's input-output function is:

$$y(t) = R_{\max}((x(t) - x_0)^2 / ((x(t) - x_0)^2 + K_m)) - 0.1, \quad x(t) \geq x_0 \quad (9)$$

$$y(t) = -0.1, \quad x(t) < x_0$$

SR is simply added to the output of this nonlinearity. Also, if SR is less than 0.1 spikes/second, the rate-function will drop below zero at times. When this happens, the output of the lowpass filter is half-wave rectified to avoid negative spike-rates; i.e. spike-rates below zero are set to zero. This model fits data from individual auditory nerve fibers, but fails to account for the population data (Fig. 6B and C). The result doesn't depend on the particular values of x_0 and K_m chosen; no single set of parameter values that could capture the population data was found (not shown).

Stimulus Description and Data Analysis

In general, modeling data are generated from, and analyzed using procedures identical to those used by Heil and Irvine in their experimental paper (Heil and Irvine, 1997). Unless otherwise indicated, the stimulus $S(t)$ was a pure tone (of duration D and peak-pressure A) presented at the CF of the auditory nerve fiber and shaped with cosine-squared or linear rise-envelopes of rise/fall-time (henceforth simply "rise-time") T ; as described further in Appendix 1. The total stimulus duration was 200 ms. Tones from 10 to 90 dB (10 dB intervals) with rise-times of 1.7, 4.2, 8.5, 17, 42, and 85 ms were presented. All computations used MATLAB 5.3.1 running on a SGI Origin 200 computer (IRIX 6.5.4). Sampling was at least 60,000 Hz, and it was always ensured that sampling at higher rates did not change results in any noticeable manner.

Responses were measured in a 210 ms trial window starting at tone-onset. As in experimental data (Heil and Irvine, 1997), all response measures were defined as the average over a set of 20 stimulus presentations. These averages were estimated by repeating this stimulus set (consisting of 20 presentations) 300 times.

Minimum experimental latency includes time for sound to reach the basilar-membrane from the speaker, basilar-membrane travel time, and delays due to transduction and axonal conduction. In Figs. 2 and 3, small time delays were added to model latencies to align their minimum value with that in experimental data (Fig. 2: 1 ms; Fig. 3: 0.7 ms). In Figs. 4, 6 and 10, model CF was fixed at 8 kHz. S and K remain almost

unaffected when CF is varied over the experimental range. Therefore a CF of 8 kHz was used while generating these population plots to avoid the computational load of the high sampling frequencies required when CF is high.

A total absolute deviation statistic (TAD) was computed to quantify the degree of fit between model and experimental mean latency data shown in Figs. 2 and 3.

$$\text{TAD} = \sum_{k=1}^n |r_k - \bar{r}_k| \quad (10)$$

where r_k is the mean latency at the k -th stimulus value, out of a total of n stimulus values. \bar{r}_k is the mean of the model's mean latency at the k -th stimulus value, estimated by averaging across 2000 repetitions of the stimulus set (which consists of 20 stimulus presentations at each stimulus value). By computing TAD for model responses to each of the 2000 repetitions, the distribution of TAD was estimated. TAD gives the amount by which the model's response to a particular presentation of the full stimulus set differs from the expected response of the model to the same stimulus-set; thus, it is a measure of the amount of deviation from the model that arises due to the intrinsic variability of the model itself. The value of the same statistic was then computed by using the experimental mean latency data; i.e. by using experimental data for r_k . Comparing the value of TAD for experimental data to the distribution of TAD values obtained by random sampling from the model shows the likelihood that a random sample drawn from the model itself (instead of from experimental data) would show the same amount of deviation as that seen in Figs. 2 and 3 between experimental and model data.

Curve-Fits and Fitting Criteria

Following the analysis of experimental data in Heil and Irvine (1997), two parametric curve fits were performed on model data. The curve

$$L = L_{\min} + 13.3/(\log(\text{MAPP}) + S)^4 \quad (11)$$

was fit to latency (L) versus $\log(\text{MAPP})$ plots. L_{\min} is the asymptotic minimum latency, and S gives "sensitivity". Latency at a given MAPP decreases as S increases, with L_{\min} constant. The curve:

$$SD = SD_{\min} - (4K(1/13.3)^{1/4}(L - L_{\min})^{5/4}) \quad (12)$$

was fit to latency versus standard-deviation (SD) plots. SD_{\min} is asymptotic minimum standard-deviation. K behaves roughly like $-1 \times$ slope of latency versus standard-deviation.

During fitting, the error function (i.e. the squared-difference between the prediction based on the fitted curve and experimental data) for each data point was weighted by the response probability (probability of ≥ 1 spike/trial, estimated from 20 trials) associated with that data point. This weighted sum of error functions across all data points was minimized to find the best fit. Fitting was done using MATLAB's *Isqcurvefit* algorithm. Curves fit data well; once data points to include in the fit were chosen (see next paragraph), the fitting procedure was uncomplicated.

The following criterion (Criterion 1) was used during experimental analysis (Heil and Irvine, 1997) to exclude low-SPL data that deviated from the common curve on which other points lay. For fibers with SR less than or equal to 0.5 spikes/second, responses within 20 dB of firing threshold (less than 50 dB SPL for the two low-SR experimental data examples illustrated) were excluded. For the others, responses whose latency or standard-deviation was larger than the minimum spontaneous latency or standard-deviation obtained from 6 no-stimulus trials were excluded. From experimental data, it appears that Criterion 1 excludes most experimental data points that deviate from the curve.

While model and experimental data mostly show excellent agreement, they do differ in one aspect. Model spontaneous latencies and standard-deviations are less variable than experimental latencies and standard-deviations and have higher values (closed symbols near the ordinate in Figs. 2B and C and 3B and C tend to lie above open symbols and are less spread out). Therefore, Criterion 1 with model spontaneous values includes many low-SPL data points that would have been excluded if experimental spontaneous values had been used. If parameter estimates from curve fitting depend on points chosen for inclusion during fitting, model and experimental parameter estimates will differ even when model and experimental responses during trials where stimuli are presented are exactly identical. As shown in Appendix 2, estimates of K are affected by this problem; i.e. K estimates are sensitive to the choice of points to include in the fit.

Therefore a different method was used to minimize, without manual intervention, the contribution to the curve fit of low-SPL data points that obviously deviated

from the curve. In this method, all responses below 50 dB SPL were excluded, independent of SR (Criterion 2). All data analysis and discussion in the main text will use Criterion 2, since it is more faithful to the spirit of the criterion used in the experimental study. Results using the original criterion (Criterion 1) are shown in Appendix 2. Criterion 1 was implemented slightly differently for model data from low-SR fibers. Since only the first-spike is modeled, and there is no way to define firing threshold in a manner similar to the experimental analysis, all responses at stimulus SPLs below 50 dB were excluded. As mentioned above, this was also the criterion used during experimental analysis of the two low-SR experimental data samples shown in Heil and Irvine (1997). It will be seen that results are qualitatively unchanged by choice of criterion; i.e. model fits experimental data well. However, population plots of model K vs. SR are more similar to K vs. SR for the experimental population when Criterion 2 is used.

Results

All experimental data and analyses are from Heil and Irvine's study of cat auditory nerve responses (Heil and Irvine, 1997), unless indicated otherwise.

Experimental Results from Individual Nerve-Fibers: Summary

Auditory nerve first-spike timing shows four properties. (1) Latency to pure tones with cosine-squared rise-envelopes decreases with SPL and depends upon rise-time. (2) Latency versus log (MAPP) curves at different rise-times align, except around low SPLs. (3) 1. and 2. are also true if one considers standard-deviation instead of latency. Thus, standard-deviation of latency to pure tones with cosine-squared rise-envelopes decreases with SPL and depends upon rise-time. Standard-deviation versus log (MAPP) curves at different rise-times align, except around low SPLs. (4) Standard-deviation of latency increases almost linearly with mean latency.

Given SR and CF, Model Data Mimics Experimental Data

The model reproduces the properties described in the preceding paragraph quantitatively. Model and exper-

imental responses for 2 fibers (with SRs of 5.8 and 52 spikes/second respectively) are shown in Figs. 2 and 3. As is the case for experimental data, model latencies decrease with SPL and depend upon rise-time (Figs. 2 and 3A). Model latency versus log (MAPP) curves at different rise-times align, except around low SPLs (Figs. 2 and 3B). Also, model standard-deviation versus log (MAPP) curves at different rise-times align, except around low SPLs (Figs. 2 and 3C). As shown in the Discussion section (also Fishbach et al., 2001), this dependence of latency and standard-deviation upon MAPP arises because stimuli with similar MAPP have very similar waveforms at onset; in other words, similar stimuli elicit similar latencies and standard-deviations.

However, the model replicates not just the dependence upon MAPP, but more importantly, also the exact nature of the dependence. Thus, model and experimental latencies for both fibers are very similar to each other (Figs. 2 and 3B); as seen by the fact that filled (model data) and open (experimental data) symbols are closely aligned, except at low SPLs. The same is true for standard-deviation (Figs. 2 and 3C). Model and experimental standard-deviations are closely aligned with each other. Finally, the relationship between latency and standard-deviation in experimental data is quantitatively reproduced by the model (Figs. 2 and 3D). This of course follows from the fact that model latencies and standard-deviations are very similar to experimental values. It will be seen from the next two sections that the nature of the dependence upon MAPP is strongly correlated with the SR (and to a lesser extent, CF) of the fiber; the model reproduces these correlations very well.

Model data do deviate from experimental data in one aspect. Model spontaneous latencies and standard-deviations are less variable than experimental latencies and standard-deviations, and have higher values (closed symbols near the ordinate in Figs. 2B and C and 3B and C lie above open symbols and are less spread out). With this exception, once SR and CF are known, the model quantitatively reproduces published experimental data from individual fibers. The good quality of the fit that is evident from visual inspection is corroborated by the TAD statistic (Methods) for the mean latency data. For both fibers, the model generated TAD values that were larger than the value obtained using the experimental mean latencies at least 75% of the time. In other words, the magnitude of the deviation seen between model and experimental mean latencies

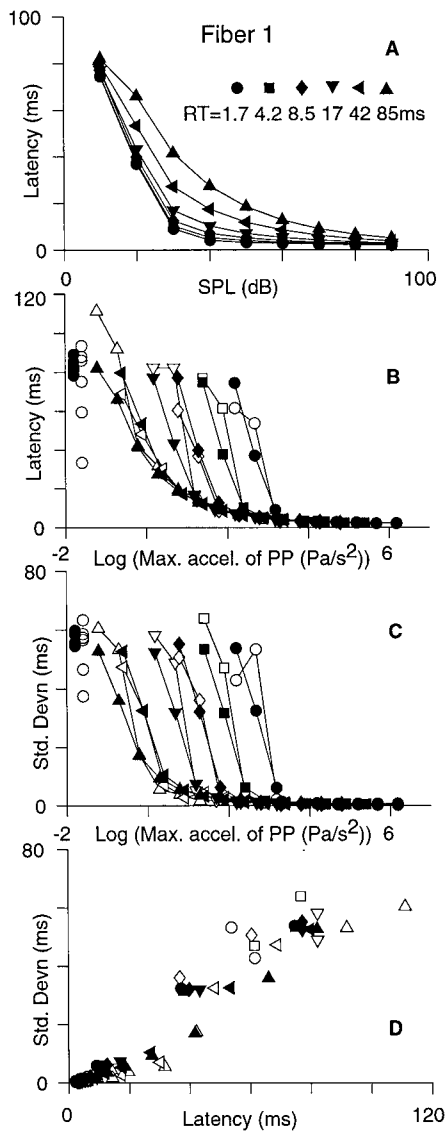


Figure 2. Model data (filled symbols) for 1 medium-SR fiber (SR = 5.8 spikes/s) show good correspondence to experimental data (open symbols: Heil and Irvine, 1997: their Fig. 2) in response to 10–90 dB CF tones with 6 cosine-squared rise-times (symbol key in A). **A:** model latency vs. SPL. **B, C:** model and experimental latency (B) and standard-deviation (C) vs. log(MAPP). Symbols near ordinate show spontaneous measures obtained from 6 trials of 20 repetitions each, where no stimulus was presented. **D:** mean latency vs. standard-deviation for experimental and model data. 1 ms was added to model latencies (see Methods). CF = 7.7 kHz.

in Fig. 2 would arise at least 75% of the time if one sampled randomly from the model. Since the standard-deviations of model and experimental data are also very similar, this behavior of the TAD statistic cannot be

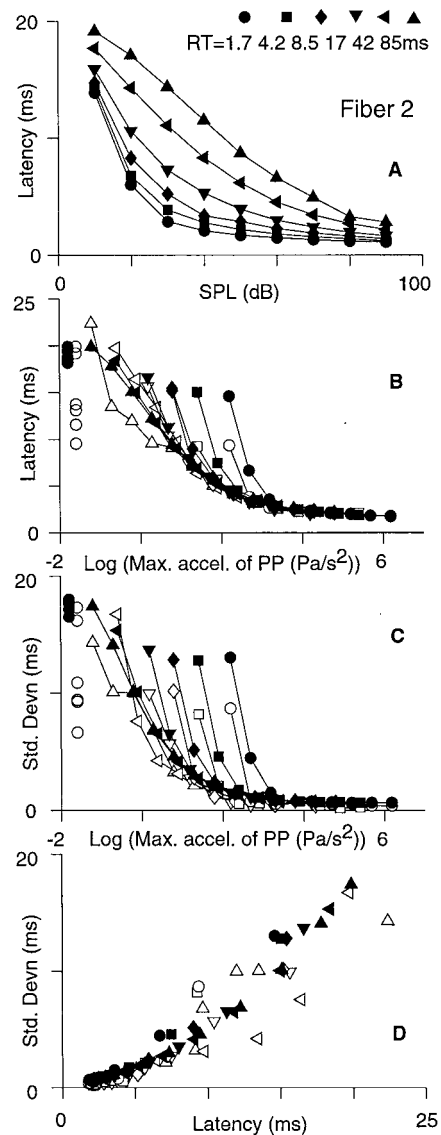


Figure 3. Another example of excellent correspondence between model and experimental data. Format as in Fig. 2, except a high-SR fiber is modeled (SR = 52 spikes/s). CF = 8.1 kHz, 0.7 ms was added to model latencies.

explained as arising from a higher variability in model responses.

It is interesting to note that in both example fibers, standard-deviation is less than the mean (Figs. 2 and 3D) at most stimulus-values and approaches the mean as mean latency becomes large. This is consistently true of both model and experimental data and can be interpreted in terms of the waiting time to first-spike for a Poisson process (see Discussion).

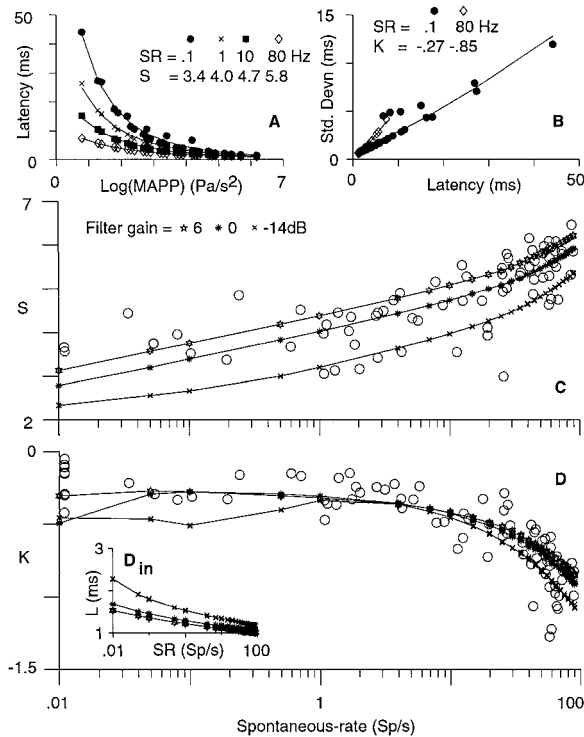


Figure 4. Model replicates SR dependence. CF = 8 kHz. **A:** Model latency vs. log(MAPP) at 4 SRs (see symbol key). The 4 solid lines are curves of the form in Eq. (11) that best fit the data at each SR. S increases with SR. **B:** Model latency vs. standard-deviation at 2 SRs. The 2 solid lines are best-fitting curves of the form in Eq. (12). K decreases with increasing SR. **C–D:** Model S , K and minimum latency (ordinates in C, D and D_{in}) vs. SR (abscissa). 3 filter gain values are used (symbol key in C). Five model S , K estimates (from five repetitions) are shown at each SR and filter gain; the line passes through their mean. Open circles (**C–D**): experimental (S , K) data.

Summary of SR Correlations Seen in the Experimental Population

Parametric curve fits were performed (Heil and Irvine, 1997) to the experimental latency versus log (MAPP) data as well as the latency versus standard-deviation data for individual nerve fibers (see Methods). The parameter estimates for these curves show strong and systematic relationships with SR. Thus, from the latency versus log (MAPP) curve fits to the population of nerve fibers, it is seen that sensitivity S increases with SR (open circles in Fig. 4C). A weak relationship has been stated to exist between the asymptotic minimum latency L_{min} and SR: L_{min} decreases with increasing SR. Finally, the slope of the latency versus

standard-deviation relationship increases with increasing SR. This leads to a lower value for the K parameter of the fitted curve as SR increases (open circles in Fig. 4D).

Model Quantitatively Reproduces These Population Properties

The experimental relationships with SR are quantitatively reproduced by the model. Figure 4A shows model latency vs. log (MAPP) data and curve fits at 4 different SRs. S increases with SR. Figure 4B shows model latency vs. standard-deviation data and curve fits at 2 SRs. K clearly decreases as SR increases. Figure 4C and D show that the similarity between model and experimental results is quantitative, and not merely qualitative. Parameter estimates from the model at different SRs are very similar to those from experimental data. The line joining the asterisks in Fig. 4C and D passes through the mean S and K parameter estimates respectively from the model (the other 2 lines are described in the next paragraph). This line closely follows the trend shown by the experimental data (open circles). Finally, model L_{min} estimates increase slightly with SR and thus fail to mimic the reported (weak) negative correlation between experimental L_{min} estimates and SR (not shown). However, a closely related quantity, model minimum latency (across all stimuli tested: Fig. 4D_{in}) clearly decreases as SR increases. This has also been seen experimentally by Rhode and Smith (1985).

There is considerable scatter in experimental S (and to a lesser extent, K) values at a given SR. However, experimental parameter estimates come from fibers with a range of CFs and from different animals. It is well-known that the gain of the external/middle-ear filter varies with frequency (Rosowski, 1991); this is considered a major determinant of the audiogram. This suggests a simple hypothesis: different external/middle-ear filter gains at different CFs as well as filtering differences across animals contribute to scatter in S . This hypothesis is strongly supported (and was motivated) by the result (Heil and Irvine, 1997) that S varies with CF in a manner that resembles the cat's audiogram (Fig. 5B).

The model fits 2 example fibers with CFs near 8 kHz without any external/middle-ear filtering (Figs. 2 and 3). Note that this is because x_0 was set to achieve this; varying x_0 is identical to changing the gain G of the external/middle-ear filter. Parameter estimates

were also obtained from the model with the parameter G set to 6 dB, 0 dB and -14 dB. These values were initially chosen because minimum and maximum thresholds over the experimental CF range (.6–35.5 kHz), relative to 8 kHz, were *roughly* -6 dB and 14 dB for the N1 audiograms in Rajan et al. (1991). The effect of the three different gain settings is simply to change the SPL of the input stimuli by 6, 0 and -14 dB respectively. The curves at the 3 filter gain settings (which are vertically displaced with respect to each other) together span most of the scatter in experimental S values, suggesting that external/middle-ear filtering may indeed explain the scatter in S .

The following analysis was then performed to examine this explanation (that scatter in S results from the CF-dependent variation in gain of the first gain stage representing external/middle-ear filtering) more directly. For each of the 77 auditory-nerve fibers in the experimental data, model CF and SR were fixed at experimental values and the gain G that produced a model S value closest to that of the experimental fiber was found. A bisection method was used to find the best-fitting G ; it guaranteed that the estimated best-fitting value of G was not farther than 0.1 from the true best-fitting value of G . The 77 estimated G values are plotted versus CF in Fig. 5A. A U-shaped relationship is visible, with minimum G values between about 15 and 30 kHz. Published psychophysical audiograms from different studies (Fay, 1988; Heffner and Heffner, 1985; Neff and Hind, 1955) as well as N1 audiograms from different cats (Rajan et al., 1991) show substantial variability; however, they are all U-shaped and the shape of these audiograms is *roughly* consistent with the shape of G vs. CF plot in Fig. 5A. For comparison, plots of S versus CF for experimental data are also shown in Fig. 5B for each of the three SR classes; as reported earlier (Heil and Irvine, 1997), a similar U-shaped relationship with CF is seen for S as well.

The above results show that the variation in population parameters with SR is reproduced very well by the model. As noted in the Methods section, since SR increases in the model are accompanied by changes in the shape of the static nonlinearity, it is not possible to disentangle their contribution to the observed correlations with SR. For example, S may increase with SR simply because higher spontaneous drives generate shorter latencies (Heil and Irvine, 1997), producing higher sensitivity. Results using an alternative model, described in the next section, help disassociate the contribution of these two factors.

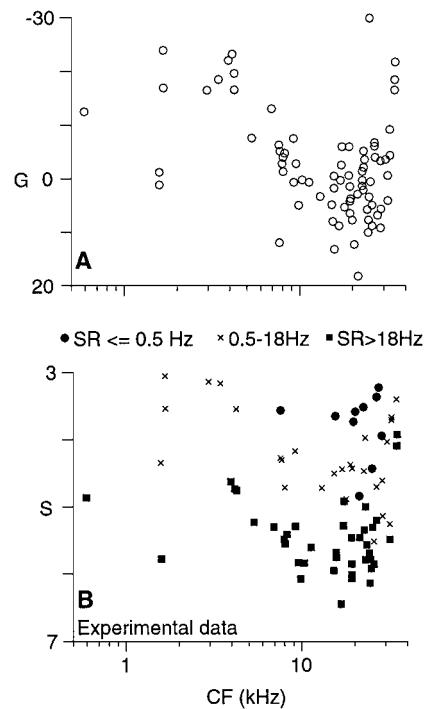


Figure 5. Model and experimental parameter dependence on CF. **A:** Plot of gain (G : estimated from experimental S values) of external/middle-ear filter stage is roughly consistent with published audiograms (see text). **B:** Experimental S vs. CF plot for comparison; experimental S values for low, medium and high-SR fibers are plotted using different symbols (see key).

Data Rule Out an Alternative Model for SR Generation

An alternative SR model assumes that SR is added to the stimulus-driven output of a fixed nonlinearity. SR generation is thus independent of the model's stimulus-driven stages (full description in Methods); in other words, SR changes are not accompanied by changes in the shape of the nonlinearity. S values from the alternative model do increase with SR, as shown in Fig. 6B. However, this increase is very small when compared to that seen in the experimental population. At higher SRs, experimental S values are much larger than model S values, independent of the filter gain settings used. The discrepancy is not because of the particular values of x_0 and K_m chosen; no single set of parameter values that could capture the population data was found (not shown). On the other hand, K estimates from the alternative model behave similar to those from the original model (Fig. 6C, solid lines follow the open circles well). Thus, while the dependence of K on SR may

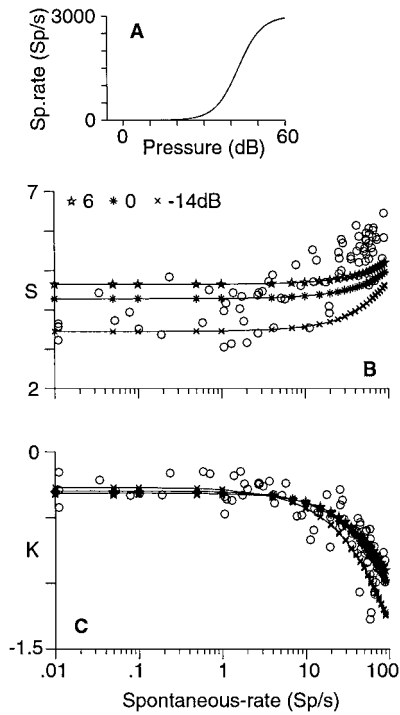


Figure 6. **A:** Input-output function of the nonlinearity used in the alternative model. *Y* axis shows spike-rate (spikes/second). **B, C** use the same format as Fig. 4C and D respectively, except that the alternative model with additive SR is used instead.

indeed result simply from the increase in SR, the dependence of S on SR in the original model arises from the variation in shape of the static nonlinearity.

Experimental Responses to Linear Rise-Envelopes in Cortex: Summary

Properties 1–4 described above for individual auditory nerve fibers in response to tones with cosine-squared rise-functions are also true for responses from auditory cortical neurons (Heil, 1997a; Heil and Irvine, 1998). In addition, a similar set of 4 properties holds for *cortical* responses to *linear* rise-envelopes (Heil, 1997a; Heil and Irvine, 1996). The 4 properties are: (1) Latency to pure tones with linear rise-envelopes decreases with SPL and depends upon rise-time. Latency versus rise-time plots at different SPLs are compressive. (2) Latency versus $\log(\text{MVPP})$ curves at different rise-times align, except at low SPLs. (3) 1. and 2. are also true if one considers standard-deviation instead of latency. Thus standard-deviation of latency to pure tones with linear rise-envelopes decreases with

SPL and depends upon rise-time. Standard-deviation versus $\log(\text{MVPP})$ curves at different rise-times align, except at low SPLs. (4) Standard-deviation of latency increases almost linearly with mean latency. Also, standard-deviation increases faster with latency in response to linear rise-envelopes, as compared to cosine-squared rise-envelopes.

Model Accounts for Responses to Linear Rise-Envelopes as Well

Auditory nerve fiber responses to tones with linear rise-envelopes have not been reported in the literature. Also, while the latency properties of cortical responses to tones shaped with linear rise-envelopes have been modeled (Fishbach et al., 2001), the properties of standard-deviation have not been modeled. The present model replicates all the properties described above for auditory cortical neurons using tones shaped with linear rise-envelopes, further supporting the idea that these cortical properties are established in the auditory nerve. This is shown in Fig. 7, where the responses of the nerve-fiber in Fig. 2 to tones with linear rise-envelopes are shown. Figure 7A shows that latency decreases with SPL and depends upon rise-time. Latency versus rise-time plots are compressive (Fig. 7E and F). Latency versus $\log(\text{MVPP})$ curves align, except at low SPLs (Fig. 7B). Standard-deviation versus $\log(\text{MVPP})$ curves also align, except at low SPLs (Fig. 7C). Standard-deviation increases almost linearly with mean latency (Fig. 7D). Finally, standard-deviation in response to tones with linear rise-envelopes increases faster with latency when compared to the standard-deviation in response to tones with cosine-squared rise-envelopes (Fig. 7D, D_{in}).

Parameter Sensitivity

Varying model CF (2 kHz to 24 kHz), lowpass filter corner-frequency (625 to 3750 Hz) and R_{max} (300 to 4500 spikes/second) has little effect on S and K estimates (data not shown). Increasing R_{max} decreases L_{min} and SD_{min} (Fig. 8) for a range of corner frequency and CF values. Effects of corner frequency and CF on L_{min} and SD_{min} are small. Thus the different curves in Fig. 8, which are derived at different corner frequencies and CFs, are only slightly different from each other. The small variation in L_{min} and SD_{min} at a given R_{max} is due to CF (not shown). Increasing CF decreases L_{min}

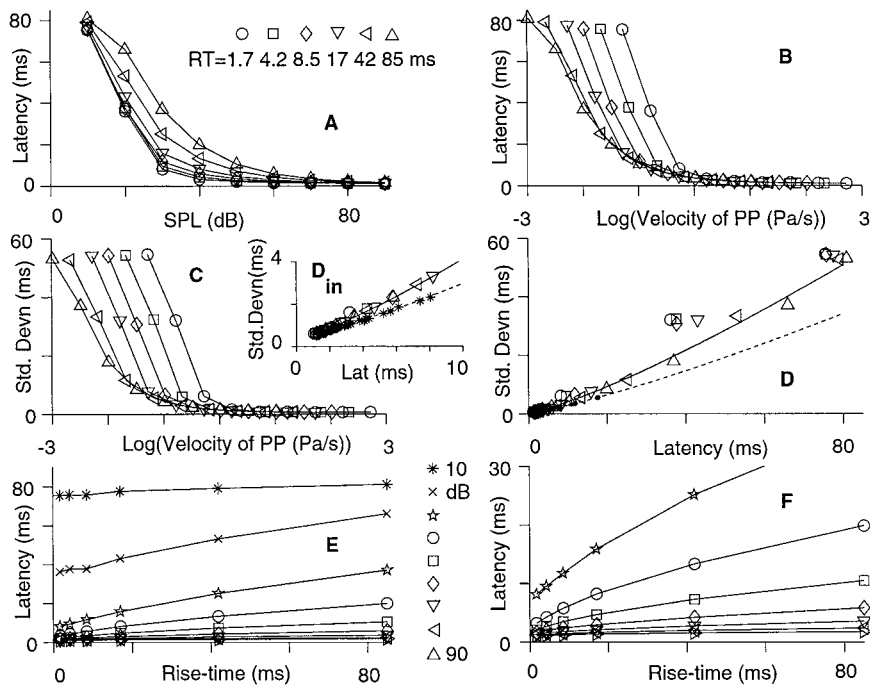


Figure 7. A–F: Predictions for Fiber 1 from Fig. 2 (SR = 5.8 spikes/second, CF = 7.7 kHz) for linear rise-envelopes (rise-times in symbol key). A: Latency vs. SPL. B, C: Latency (B) and standard-deviation (C) vs. log(MVPP). D: Standard-deviation vs. latency. Solid line is best latency vs. standard-deviation curve fit. Dashed line is similar, except responses using cosine-squared rise-envelopes (asterisks; identical SPLs and rise-times) are fit. Inset to D (D_{in}) shows D magnified around the origin. Standard-deviation increases faster with latency for linear than for cosine-squared rise-envelopes. E: latency vs. rise-time (10–90 dB SPL; symbol key between E and F) plots are compressive. F: E shown at a higher ordinate resolution.

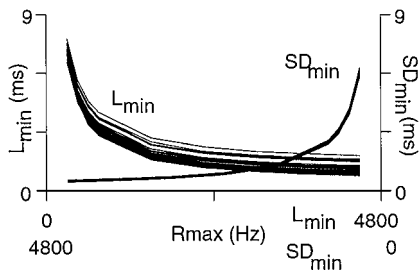


Figure 8. Sensitivity of results to variations in model parameters. L_{min} (left Y axis, X axis increasing from left to right) and SD_{min} (right Y axis, X axis decreasing from left to right) vs. R_{max} , at 36 different CF-corner frequency combinations: 6 CFs (2, 4, 8, 12, 16 and 24 kHz) and 6 corner frequencies (625, 1250, 1875, 2500, 3125, and 3750 Hz). SR was 5 spikes/second.

slightly, as expected from the properties of the gamma-tone filter (Methods).

Discussion

The model used in this paper (henceforth “the present model”) accounts quantitatively for almost all of the

experimental data on first-spike timing, its variability, and their relationship to SR. The results can be divided conceptually into four parts: (1) Modeling the dependence of mean latency upon MAPP and MVPP, the exact nature of that dependence, and its systematic variation between fibers. (2) Modeling the dependence of standard-deviation upon MAPP and MVPP, the almost linear relationship of standard-deviation to the mean, and the systematic differences in the slope of this relationship between different fibers. (3) Modeling the effects of SR (both trend and scatter) on the envelope-dependence of latency and standard-deviation. (4) The physiological mechanisms that underlie the above results. In addition, based on the present model, one can provide answers to questions raised by the data. For example, does the SR dependence reveal anything about the structure of the system, or is it a mere consequence of the variation of baseline firing rate with SR? Are the differences seen in the response properties of cortical and nerve fiber populations the result of intermediate transformations, or can they be simply explained by the different SRs in these 2 areas?

Comparison of Three Different Models

The present model passes the stimulus through a gain stage, a bandpass filter, a rectifying, saturating non-linearity, and a lowpass filter connected in series and then uses the output of this series combination to drive an inhomogeneous Poisson process. Such a model is consistent with many previous models of auditory nerve responses (see Methods). The model has two variable parameters. One parameter controls the shape of the nonlinearity and is determined by SR. The other parameter models the CF-dependent gain of the gain stage, which represents the external/middle-ear filter. The results are shown to be quite insensitive to variations in the other (fixed) parameters. The inhomogeneous Poisson process that is used to generate a spike functions by integrating the lowpass filter output and generating a spike when the integral crosses a random threshold that is exponentially distributed with mean 1.

Two other recent models are relevant to this discussion. The first model (Fishbach et al., 2001) accounts qualitatively for various properties of *mean* latency and onset response magnitude in the *central* auditory system. In Fishbach et al.'s model, the auditory nerve response is obtained by lowpass filtering a log-compressed version of the amplitude envelope of the stimulus. The output of the auditory nerve is then passed through a series of stages that consist of further lowpass filtering, compression, and bandpass filtering, followed by a leaky integrate-and-fire spike-generator that gives the central auditory response. The stages that follow the auditory nerve essentially serve to reproduce the result that the onset response magnitude in the central auditory system often increases non-monotonically with SPL at short rise-times and monotonically at longer rise-times. Fishbach et al. show that mean latency in their model depends on MAPP/MVPP and use their model to correctly explain the reasons for this dependence in the experimental data. However, the model fails to reproduce the exact form of the dependence on MAPP/MVPP seen in experimental latency data. As the authors point out, the model markedly underestimates experimentally measured mean latency values, and generates S values that are consistently higher than those measured experimentally. This departure is likely to be even more severe if one uses the output of the auditory nerve stage directly to generate a spike, for reasons discussed below. Also, the stochastic nature of latency is not modeled; the model treats latency as depending deterministically on the stimulus. Finally, since the fo-

cus of the model is on central auditory responses, the SR dependence in the auditory nerve is not considered either. In fact, SR in the model is always zero.

The other model, which was developed concurrently with the present model, is that of Heil and Neubauer (2001). In contrast to Fishbach et al.'s model, Heil and Neubauer's model considers mean latency at the level of the auditory nerve. However, as in the Fishbach et al. model, latency is treated as a deterministic quantity and its stochastic nature is not modeled. Heil and Neubauer's model treats the auditory nerve response as being the result of integrating (with a constant leak) the stimulus' amplitude envelope. The equation $\int_0^{L-L_{\min}} (P - P_c) dt = T$ is used to model the data, where P is the peak-pressure waveform, L the measured latency, and P_c , T and L_{\min} are free parameters estimated for each neuron by least-squares fitting its latency data. The first-spike is generated when the integral crosses the threshold value T (that varies from fiber to fiber). Their model provides excellent fits to the experimental mean latency data, after excluding response latencies that are close to or larger than spontaneously measured values. Also, the threshold and leak parameters obtained by fitting the latency data are well correlated with the experimentally measured SR. However, the SR predicted by the model is consistently and markedly lower than experimental SR by an average of about 25 spikes/second. The authors argue that this reflects a base rate of about 25 spikes/second to which the spike-rate generated by their model is added; it is not clear why this base-rate is not accounted for directly by the P_c parameter. Further, even after incorporating a base-rate of this magnitude, predicted SR is often negative (up to about -65 spikes/second) in low-SR fibers.

Heil and Neubauer visualize their integrator as operating via the integration of calcium currents at presynaptic sites in the inner hair cell. They postulate a calcium influx into the presynaptic site that is proportional to peak-pressure; when the intracellular calcium reaches a threshold concentration, the spike is generated. Studies of vesicle exocytosis in the auditory nerve synapse (Beutner et al., 2001; Moser and Beutner, 2000) do not show any evidence for the existence of such an integration stage. More importantly, this mechanism (at least as described in their paper) is clearly inconsistent with the high-frequency response properties of this synapse. The auditory nerve synapse can synchronize to stimulus frequencies up to 5 kHz (Weiss and Rose, 1988); the long time-constant of the calcium concentration

in their model will filter out frequencies much lower than this. It may be possible to rescue the mechanism by additionally postulating that the accumulated *presynaptic* calcium is rapidly buffered away once the threshold concentration is reached; in other words, the calcium concentration is reset to baseline once the spike is generated. This is only a hypothetical possibility; the synchronization properties of such “integrate-and-fire with reset” models under different stimulation conditions and parameter settings remain a subject for study (e.g. Brunel et al., 2001). Moreover, no physiological basis is known for such a buffering mechanism. In the present model, the integrator stage instead emerges naturally from the standard stochastic model of the auditory nerve spike-train as arising from a Poisson spike-generating process.¹ The Poisson process, modified by a refractory-period, is commonly used in auditory nerve models (e.g. Carney, 1993; Hewitt and Meddis, 1991) and analyses of auditory nerve data (e.g. Gaumont et al., 1983; Johnson, 1978); this is mostly motivated by the exponential nature of the inter-spike interval distribution. The high-frequency response properties of the Poisson process are also fully consistent with the ability of auditory-nerve fibers to follow high-frequency stimuli, as discussed further in a following section. Finally, the Poisson process can be shown to be the limiting distribution for sums of independent random point processes under very general conditions (Daley and Vere-Jones, 1988). Indeed, the Poisson process is the “standard” way to model spike-trains, both in the auditory system and in the rest of the brain (Johnson, 1996; Rieke et al., 1997).

For all of the reasons mentioned above, and because the present model is more consistent with existing models of auditory nerve function, it is arguable that the present model is the best available way to account for Heil and Irvine’s data. Further, because it explicitly models the envelope extraction stage, the present model can be naturally extended to low-frequency tones or to more complex signals, where it is not possible to simply consider the peak pressure waveform as driving auditory nerve responses. Incidentally, it is interesting to note that the stochastic nature of the present model (unlike the other two models) is an advantage not only because it accounts for the properties of standard-deviation, but also because it allows the plausible and physiologically-consistent interpretation of the integration stage as arising from Poisson spike-generation.

Dependence Upon SR

Fibers of different SR can receive input from the same inner hair cell (Liberman, 1982; Liberman et al., 1990; Merchan-Perez and Liberman, 1996). Therefore, the variation in shape of the static nonlinearity and the resulting change in resting bias that produces the variation in model SR may both arise from the process that converts inner hair cell potential to spikes (i.e. from the synaptic input-output function). This synaptic input-output function is affected by a wide range of pre- and post-synaptic factors, including those related to calcium dynamics, vesicle release, and post-synaptic receptor properties. The resting-bias mechanism for SR has also been proposed on the basis of other results from the auditory nerve (Horst et al., 1990; also: Yates, 1991). In the present model, the shape of the nonlinearity is fully determined by SR. An alternative model where SR is simply added to the stimulus-driven output of a fixed nonlinearity captures the dependence of K on SR, but clearly fails to replicate the dependence of S on SR. This suggests that the dependence of S on SR is not simply the result of an increased baseline firing rate at higher SRs, but actually reflects some SR-dependent structural property of the auditory periphery. More specifically, in terms of the model, it reflects the shape of the peripheral static nonlinearity. Incidentally, the fact that pure tones presented away from CF can suppress SR in auditory nerve fibers also suggests that SR is influenced by the stimulus, and is not separate from the stimulus-driven stages of the system (Henry and Lewis, 1992). SR is also inversely proportional to firing threshold, and it has been suggested that this is because low-SR fibers have lower slopes in their input-output function around firing threshold (Geisler et al., 1985). The model shares this property. However, in order to make direct quantitative comparisons to threshold data, it would be necessary to extend the model to steady-state responses by including one or more stages of adaptation (e.g. Hewitt and Meddis, 1991).

Discrepancies Between Model and Experiment

Model spontaneous measures are larger and less variable than those observed experimentally, even when SRs are identical. The experimental distributions for the spontaneous measures are broader, and have a longer tail at the low end (thus generating lower spontaneous values for mean and standard-deviation) when compared to model distributions at the same SR. This

may be the result of the fact that, unlike in the model, experimental spontaneous firing is not strictly Poisson (see Lowen and Teich, 1992).

While experimental L_{\min} values show a weak negative correlation with SR, model L_{\min} values using Criterion 2 actually show a slight positive correlation. This discrepancy is likely to be an artifact of the differences in fitting procedure, because model L_{\min} values using Criterion 1 do decrease with increasing SR, as seen experimentally. Thus, L_{\min} appears to be quite sensitive to the choice of points to include while fitting. Further, a more robust measure of model latency, the minimum latency across all stimuli tested, showed a clear negative correlation with SR; this has also been seen in other experimental data (Rhode and Smith, 1985). In the experimental analysis (Heil and Irvine, 1997), this same measure shows a very strong correlation with L_{\min} , and is therefore also expected to show the same negative correlation with SR as L_{\min} . These results give further credence to the possibility that the failure of Criterion 2 L_{\min} values from the model to show the negative correlation is the result of some artifact of the Criterion-2 based fitting procedure.

Occasional low-SR fibers have long minimum latencies (Heil and Irvine, 1997; Rhode and Smith, 1985). Low-SR fibers may have smaller maximal firing rates (Lieberman et al., 1990; but see: Yates, 1991). If so, model R_{\max} may be smaller (than the 3000 spikes/second value used in the present model) for these low-SR fibers. This would explain the longer minimum latencies, because L_{\min} increases with decreasing R_{\max} (Fig. 8).

Dependence Upon CF

Estimates of the parameter G from the experimental data reveal a U-shaped dependence of G on CF (Fig. 5A). Published psychophysical audiograms from different psychophysical studies (Fay, 1988; Heffner and Heffner, 1985; Neff and Hind, 1955) as well as N1 audiograms from different cats (Rajan et al., 1991) show substantial variability. Given this variability, the observed relationship between G and CF is roughly similar to these audiograms; this supports the hypothesis that the scatter in S at a given SR can be accounted for by considering the effects of CF-dependent external/middle-ear filtering. Experimental S estimates also depend on CF in a manner roughly resembling the audiogram (Fig. 5B); the scatter in S at a given CF arises at least partly from the variation in SR at a given

CF. In the ideal situation (where the model accounts perfectly for the data), if all the variation at a given CF in the S vs. CF plot (Fig. 5B) were due to SR, then model G estimates should be constant at a given CF. This is because the parameter G depends only on CF, and not on SR; thus, estimating G should factor out the influence of SR in the S vs. CF plot. Considerable variability in G still remains at most CFs. This variability could of course arise from across-animal differences in filtering as well as other sources of noise. The variability could also arise from the fact that in the model, x_0 was kept fixed as SR varied; only K_m was allowed to vary with SR. Any variation in the shape of the nonlinearity that is not captured by varying K_m will affect the G estimate. It would be interesting to reexamine these issues in data derived from a single animal.

Dependence of Latency Upon MAPP/MVPP

As shown by Fishbach et al. (2001), the dependence of mean latency on MAPP/MVPP arises because stimuli with similar MAPP/MVPP are similar at onset. Linear rise-envelope tones with equal MVPP are identical during their rise-time (see formulae in Methods). Cosine-squared rise-envelope tones with the same MAPP have similar onset-shapes (Fig. 1 in Heil, 1997b), because MAPP is the first-order Taylor series approximation at onset for cosine-squared rise-envelopes (Fishbach et al., 2001). Similar stimuli will elicit similar responses; therefore, *any* model that generates a spike based on the onset portion of the envelope will replicate the dependence upon MAPP/MVPP. Low-SPL responses deviate from the common curve on which other responses lie, because the onset ramps of low-SPL stimuli are short and their waveforms deviate early from higher-SPL stimuli with the same MAPP/MVPP (Fishbach et al., 2001); further, first-spikes at low SPLs are strongly SR-driven. This explanation is corroborated by the fact that responses at low SPLs are very similar at all rise-times (Figs. 2 and 3A).

Importance of the Integration Stage

Model S values from Fishbach et al.'s model are consistently higher than cortical experimental S values, because model latencies tend to be considerably shorter than experimental latencies. This discrepancy between model and experimental S values will be exacerbated

if one considers the response at the level of the nerve. Processing in the Fishbach et al. model at the auditory nerve stage consists of logarithmic compression and lowpass filtering. The time-constant of this lowpass filtering stage lies in the millisecond range. Indeed, the ability of auditory nerve fibers to follow pure tones up to 5 kHz limits the time-constants of the stages preceding spike-generation in any realistic model, to values in the millisecond or sub-millisecond range. Since the ability of a lowpass filter to delay a signal is limited by its time-constant, models that rely solely on static nonlinearities and lowpass filtering using a time-constant of this magnitude will fail to reproduce the data. Both Heil and Neubauer's model and the present model can reproduce latencies quantitatively, because they possess an integration stage that provides the long time-constant required to capture the latency data accurately. In the present model, this integration stage resides at the level of spike-generation; the presynaptic locus that was proposed by Heil and Neubauer for their integration mechanism is not consistent with the ability of auditory nerve-fibers to follow high-frequency tones, as argued in a previous section. Long time-constants in the spike-generation stage can co-exist with an ability of the spike-train to follow high-frequency input. Indeed, the Poisson spike-generator can follow arbitrarily high frequencies; this follows immediately from the fact that it is a memoryless point process. Thus, numerous models for phase-locking to pure tones in the auditory nerve use Poisson spike-generators successfully (e.g. Carney, 1993; Hewitt and Meddis, 1991). Fishbach et al.'s model uses a leaky "integrate-and-fire" spike-generator, which operates as a threshold applied to the output of a first-order lowpass filter. Simulations (unpublished observations) suggest that one would have to use a very long time-constant for the spike-generator's lowpass filter in order to reproduce the latency data accurately using their model. However, in reality, this time-constant is limited physiologically by the membrane time-constant and therefore, it appears unlikely that the membrane time-constant is long enough to be the source of the long latencies seen in experimental data (Heil and Neubauer, 2001). Further, in contrast to the situation with the Poisson spike-generator, the ability of integrate-and-fire spike-generators to follow high-frequency stimuli under different stimulation conditions and parameter settings remain a subject for study (e.g. Brunel et al., 2001).

A Threshold Model is Not Ruled Out

A simple model for first-spike generation suggests that the first-spike is generated when stimulus amplitude crosses a fixed threshold value. This model has been rejected for 2 reasons (Heil and Irvine, 1997; also see Heil and Neubauer, 2001). However, the latency data can be reproduced using a threshold that acts on a transformed version of the stimulus envelope. The 2 reasons for rejecting the stimulus threshold model were: (1) Consider a linear rise-envelope $E(t) = t/T$ (T : rise-time), and a threshold B . If latency L is the envelope's threshold-crossing time, then $L = BT$; L is linearly related to T . Experimental latency versus rise-time plots are instead compressive (Heil and Irvine, 1996). To see why applying the threshold to the integrated envelope produces compressive plots, consider the following argument. Assume that the first-spike is generated when the integral of the (linear) rise-envelope $E(t)$ crosses a threshold B ; L is the time of threshold-crossing (first-spike latency). Then:

$$\int_0^L E(t) dt = \int_0^L (t/T) dt = L^2/(2T) = B; \quad (13)$$

Solving, $B = L^2/(2T)$, $L = \sqrt{2BT}$

L is thus a compressive function of T . (2) If the stimulus threshold model were valid, peak pressure at the time of spike-generation τ (estimated as latency predicted from the latency versus log(MAPP) curve fit minus L_{\min}) would be identical to threshold peak pressure, and therefore constant. Experimental data from primary auditory cortical neurons contradicts this (Heil, 1997b). In primary auditory cortex, peak pressure at the end of an "integration period" (response latency predicted from latency vs. log(MAPP) curve fit for each stimulus presented minus L_{\min} ; this is the same as τ) is not constant, and has a characteristic pattern (Heil, 1997b, Fig. 8). The present model predicts that auditory nerve fibers will also show this characteristic pattern, as shown for the response of the fiber in Fig. 2 (Fig. 9). Again, this is because the threshold acts on a transformed version of the stimulus. The transformation process introduces an envelope-dependent delay, i.e. the spike is generated after different amounts of delay for different stimuli. Subtracting a constant L_{\min} will not compensate for this stimulus-dependent delay. Estimation errors in L_{\min} can further accentuate the effect.

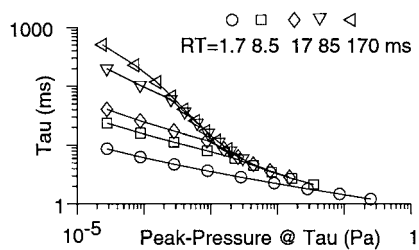


Figure 9. Plot of “integration period” τ vs. peak pressure at τ for Fiber 1 from Fig. 2 replicates pattern reported for auditory cortical neurons. Stimulus duration = 400 ms. A cosine-squared rise-envelope, and SPLs from 10–90 dB at 5 different rise-times (symbol key) were used.

Variability of First-Spike Timing

Phillips and colleagues pointed out that the mean standard-deviation of first-spike timing in auditory cortical neurons is less than a millisecond (Phillips and Hall, 1990). This surprisingly low variability is comparable to that found in the auditory nerve (Heil, 1997a; Heil and Irvine, 1997; Phillips and Hall, 1990). At both loci, standard-deviation of latency increases almost linearly with mean latency. The standard-deviation of the latency distribution predicted by the present model, once SR and CF are known, agrees excellently with experimental standard-deviations. The present model uses a Poisson spike-generator; spike-timing from this generator can be interpreted in terms of the time to cross an exponentially distributed threshold. As is often pointed out, the decrease in standard-deviation of latency with a decrease in mean latency is probably related to the fact that functions with steep slopes cross (random) thresholds early (giving a smaller mean latency) and quickly (resulting in a smaller jitter in threshold-crossing time: e.g. Cecchi et al., 2000; Stein, 1967). Interestingly, very similar results have emerged from studies of the visual system. Spike-timing in response to transients can be extremely precise. Further, both variability and latency decrease with stimulus magnitude (e.g. Berry et al., 1997); however, the relationship between these two measures doesn't seem to have been examined.

The model also accurately accounts for the dependence of standard-deviation upon SR for the auditory nerve population. For a given latency, standard-deviation is higher if SR is higher. A very similar result has been obtained recently for first-spike latency in integrate-and-fire models (Van Rossum, 2001) under a wide range of stimulation conditions. The author shows

that background noise (which would also increase SR) decreases first-spike latency and increases standard-deviation, thus producing a fast but jittery response. Interestingly, background noise is also reported to improve the sensitivity of neurons to small inputs (Ho and Destexhe, 2000). This result is reminiscent of the lower thresholds in high-SR fibers. These analogies hint at possible general principles in the relationship between SR and transient responses in the nervous system.

S and K: Effects of Central Processing?

S values from auditory nerve and primary auditory cortex largely overlap (Heil and Irvine, 1997); however, the very large S values seen in the nerve are not seen in the cortex. Also, auditory cortical neurons do not show a large part of the range of small K values that are found in the nerve. It has been suggested that these differences might arise simply from the lower SR in anesthetized auditory cortex as compared to the nerve (Heil and Irvine, 1997). The modeling results support this suggestion. The difference between the largest S values seen in nerve and cortex is about 0.9 (Heil and Irvine, 1997). This is not much larger than the variations of S with SR at a given filter-gain (Fig. 6B) for the alternative model. Similarly, by comparing responses from the alternative model to those using the present model, it can be seen that the dependence of K on SR primarily reflects the baseline firing rate.

Factors like best modulation-frequency (e.g. Krishna and Semple, 2000) and stimulus location (e.g. Brugge et al., 1996) are known to affect latency at central levels. It is not clear if these factors simply add fixed delays (which would leave S unchanged), or whether they affect the dependence of latency on MAPP/MVPP, or both (see Eggermont, 1998).

Time-Intensity Trading: A Speculation

On the basis of psychophysical data that indicate two different time-intensity trading ratios for pure tones, it has been proposed (Hafter and Carrier, 1972) that there exist two different processes for intensity-to-time conversion in the auditory periphery. It was speculated that these two mechanisms resided in the inner and outer hair cells respectively. In a model where spikes are generated when the hair cell potential crosses a threshold value, if the inner and outer hair cell thresholds were no more than 20 dB apart, the data could be accounted for. In hindsight, it seems more

plausible now to locate the two mechanisms in fibers of low and high SRs. Auditory nerve fibers have a bimodal SR distribution (Lieberman, 1978). Further, as discussed above, the sensitivity of auditory nerve fiber latencies to changes in stimulus SPL (at a given rise-time) depends on SR. This could potentially create two different intensity-to-time conversion mechanisms. The model discussed here can be used to predict the relationship between tone intensity and the distribution of first-spike latency, once SR and CF are known. It would therefore be interesting to use the present model as a starting point to try and account for psychophysical results on time-intensity trading.

Appendix 1

The stimulus $S(t)$, a pure tone with rise-time T and total duration D is described by:

$$S(t) = E(t)(A \sin(\omega t)), \quad \omega = 2\pi(CF),$$

$$A \text{ is peak pressure (Pa)} \quad (14)$$

For cosine-squared rise-envelopes:

$$E(t) = (1 - \cos(\pi t/T))/2, \quad t \leq T \quad (15)$$

$$E(t) = 1, \quad T < t \leq D - T$$

$$E(t) = (1 - \cos(\pi(D - t)/T))/2, \\ D - T < t \leq D$$

$$\text{MAPP} = A(\pi/T)^2/2 \quad (16)$$

For linear rise-envelopes (Fig. 9A–F):

$$E(t) = t/T, \quad t \leq T \quad (17)$$

$$E(t) = 1, \quad T < t \leq D - T$$

$$E(t) = (D - t)/T, \quad D - T < t \leq D$$

$$\text{MVPP} = A/T \quad (18)$$

Appendix 2

For completeness, results using Criterion 1 are shown in Fig. 10. Criterion 1 S estimates (Fig. 10A) from the present model are quite similar to experimental estimates (and therefore also to those using Criterion 2, Fig. 4C). Similarly, Criterion 1 S estimates from the alternative model (Fig. 10C) behave similar to those using Criterion 2 (Fig. 6B). Thus the estimate of S is quite robust and insensitive to the choice of data points to include in the fit. Estimates of model K values using

Criterion 1 from the present (Fig. 10B) and alternative models (Fig. 10D) are often lower than experimental K values; they are also more variable. However, they do reproduce the qualitative trend shown by Criterion 2 estimates: model K values from both the present and alternative model show an SR dependence similar to that of experimental K estimates. Finally, model L_{\min} values from the present model (Criterion 1) decrease with increasing SR as seen experimentally (not shown).

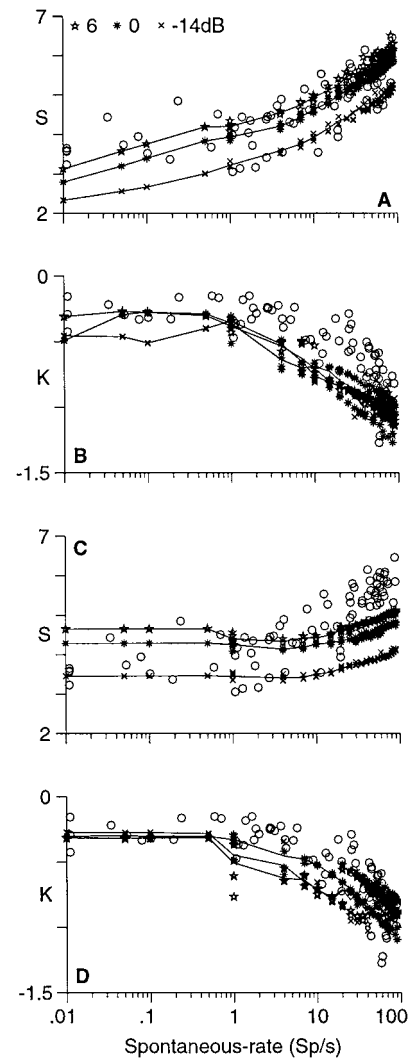


Figure 10. Plots of S and K (estimated using Criterion 1) vs. SR for both the original model where the nonlinearity varies with SR (A, B) and the alternative model with additive SR (C, D). A, C: S vs. SR, format as in Fig. 4C. B, D: K vs. SR, format as in Fig. 4D. Results remain qualitatively unchanged with this criterion; however, fits of K vs. SR are better using the modified criterion (Figs. 4 and 6).

Appendix 3

A Short Result on the CV of an Inhomogeneous Poisson Process

A quantity that relates standard-deviation and mean latency is the coefficient of variation (CV: standard-deviation divided by the mean) of the latency distribution. The CV for a homogeneous Poisson process is 1. The CV is an index of *regularity*; thus, large CVs indicate irregular processes (Johnson, 1996). The CV for both experimental and model data lies mostly below 1 (Figs. 2D and 3D). It is shown here that for the class of monotonically varying rate-functions, the CV of an inhomogeneous Poisson process is related to whether the rate-function is increasing or decreasing. Monotonically increasing rate-functions always produce CVs ≤ 1 . This is an interesting point-process analog of the notion that sharply rising waveforms elicit precisely timed spikes. The result suggests that standard-deviations in Figs. 2D and 3D are generally smaller than the means (and therefore the CVs below 1), because of the rising-nature of the stimulus envelope. The standard-deviations in Figs. 2D and 3D are also seen to become close to the mean latencies (and the CVs close to 1) when the mean latencies become long. This is because the first-spike is then strongly influenced by the final steady-state portion of the envelope (and the SR, especially at low SPLs). Therefore, the CVs become close to the value of 1 for the homogeneous process. It is also shown that monotonically decreasing rate-functions (such as might occur at the offset of a stimulus) produce CVs ≥ 1 . This is interesting because it is stated (Johnson, 1996) that while it is theoretically possible for CV to exceed 1, CVs near 1 are usually taken as an indication of irregularity. The result gives a whole class of (monotonically decreasing) rate-functions that result in a CV ≥ 1 . The proof follows.

Let $\lambda(s)$ be the rate-function for a spike train that is an inhomogeneous Poisson process. $\lambda(s) \geq 0$. By defining $f(t) = \int_0^t \lambda(s) ds$, one can show that the probability-density function $p_T(t)$ for the waiting time T to the first spike (first-spike latency) is $f'(t)e^{-f(t)}$ (Snyder and Miller, 1991). This implies that:

$$\int_0^\infty f'(t)e^{-f(t)} dt = 1 \quad (19)$$

It is well-known that the CV of T in the homogeneous case where $\lambda(s)$ is constant is equal to 1 (Snyder and Miller, 1991). It is shown here that $CV \leq 1$ if $\lambda(s)$

is monotonically increasing and ≥ 1 if $\lambda(s)$ is monotonically decreasing. To prove the case where $\lambda(s)$ is monotonically increasing, assume without loss of generality that the mean of T , $E(T) = 1$. Then to prove that $CV(T) \leq 1$, one has to show that $\text{variance}(T) \leq 1$, which is the same as showing that $E(T^2) \leq 2$ (since $E(T^2) = \text{Variance} + E(T)^2$).

$$E(T) = 1, \text{ implies that } \int_0^\infty t f'(t) e^{-f(t)} dt = 1 \quad (20)$$

Expanding by parts, and using the fact that $te^{-f(t)}|_0^\infty = 0$, one gets

$$\int_0^\infty e^{-f(t)} dt = 1. \quad (21)$$

If $E(T^2) \leq 2$, $\int_0^\infty t^2 f'(t) e^{-f(t)} dt \leq 2$. Expanding by parts as above gives

$$\int_0^\infty te^{-f(t)} dt \leq 1. \quad (22)$$

Thus, (22) must be shown to be true to get the desired result. To prove (22), consider (20). It can be shown that $\text{covariance}(Xf(X)) \geq 0$, where X is any random variable and $f(X)$ is a monotonically increasing function of X . This is intuitively seen by considering that

$$\begin{aligned} \text{covariance}(Xf(X)) &= E[(X - E(X)) \\ &\quad \times (f(X) - E(f(X)))] \quad (23) \end{aligned}$$

Clearly, the right-hand-side of (23) is ≥ 0 for monotonically increasing $f(X)$. Also, the right-hand-side of (23) can be rewritten as $E(Xf(X)) - E(X)E(f(X))$. Then $\text{covariance}(Xf(X)) \geq 0$ implies that $E(Xf(X)) \geq E(X)E(f(X))$. Using this result on the left-hand-side of (20) by treating t as X , $f'(t)$ as $f(X)$ and $e^{-f(t)}$ as the density (allowed because $0 \leq e^{-f(t)} \leq 1$ and $\int_0^\infty e^{-f(t)} dt = 1$ from (21)) gives:

$$\begin{aligned} &\int_0^\infty t f'(t) e^{-f(t)} dt \\ &\geq \int_0^\infty t e^{-f(t)} dt \int_0^\infty f'(t) e^{-f(t)} dt \quad (24) \end{aligned}$$

Substituting (19) and (20) in (24) gives $\int_0^\infty te^{-f(t)} dt \leq 1$. This is the required result.

Similarly, using the fact that if $f(X)$ is a monotonically decreasing function of X , $\text{covariance}(Xf(X)) \leq 0$; one can show that $CV(T) \geq 1$ if $\lambda(s)$ is monotonically decreasing.

Acknowledgments

Peter Heil for readily answering questions, and graciously contributing raw data. Prof. S.R.S. Varadhan for outlining the proof of the conjecture in Appendix 3. Malcolm Semple for generous contribution of lab facilities, and comments. Tony Movshon for nice, fast computers.

Note

1. Interestingly, Heil and Neubauer's model can be shown to have a form that is quite similar to that of the present model. Clearly, their model equation can be rewritten as $\int_0^{L-L_{\min}} H(P - P_c) dt = 1$, $H = 1/T$. Now, the threshold in their model is fixed (at 1) across all neurons, as in the present model. Instead, the slope of the linear input-output function varies systematically between neurons, with high-SR neurons having higher slopes. It may be possible to extend their model to the standard-deviation results by making the threshold an exponentially distributed random variable. Such a reformulation allows one to interpret the Heil and Neubauer integrator also as resulting from the Poisson spike-generating process, thus avoiding the problems associated with interpreting the integration as resulting from a process of presynaptic calcium accumulation.

References

- Anzai A, Ohzawa I, Freeman RD (2001) Joint-encoding of motion and depth by visual cortical neurons: Neural basis of the Pulfrich effect. *Nat. Neurosci.* 4: 513–518.
- Bair W (1999) Spike timing in the mammalian visual system. *Curr. Opin. Neurobiol.* 9: 447–453.
- Berry MJ, Warland DK, Meister M (1997) The structure and precision of retinal spike trains. *Proc. Natl. Acad. Sci. USA* 94: 5411–5416.
- Beutner D, Voets T, Neher E, Moser T (2001) Calcium dependence of exocytosis and endocytosis at the cochlear inner hair cell afferent synapse. *Neuron* 29: 681–690.
- Brugge JF, Reale RA, Hind JE (1996) The structure of spatial receptive fields of neurons in primary auditory cortex of the cat. *J. Neurosci.* 16: 4420–4437.
- Brunel N, Chance FS, Fourcaud N, Abbott LF (2001) Effects of synaptic noise and filtering on the frequency response of spiking neurons. *Phys. Rev. Lett.* 86: 2186–2189.
- Carney LH (1993) A model for the responses of low-frequency auditory-nerve fibers in cat. *J. Acoust. Soc. Am.* 93: 401–417.
- Cecchi GA, Sigman M, Alonso JM, Martinez L, Chialvo DR, Magnasco MO (2000) Noise in neurons is message dependent. *Proc. Natl. Acad. Sci. USA* 97: 5557–5561.
- Cooper NP, Robertson D, Yates GK (1993) Cochlear nerve fiber responses to amplitude-modulated stimuli: Variations with spontaneous rate and other response characteristics. *J. Neurophysiol.* 70: 370–386.
- Daley D, Vere-Jones D (1988) *An Introduction to the Theory of Point Processes*. Springer, Berlin.
- Dallos P, Cheatham MA (1989) Nonlinearities in cochlear receptor potentials and their origins. *J. Acoust. Soc. Am.* 86: 1790–1796.
- David EE, Guttman N, VanBergeijk WA (1959) Binaural interaction of high-frequency complex stimuli. *J. Acoust. Soc. Am.* 31: 774–782.
- Eggermont JJ (1998) Azimuth coding in primary auditory cortex of the cat. II. Relative latency and interspike interval representation. *J. Neurophysiol.* 80: 2151–2161.
- Fay RR (1988) *Hearing in Vertebrates: A Psychophysics Databook*. Hill-Fay Associates, Winnetka, IL.
- Fishbach A, Nelken I, Yeshurun Y (2001) Auditory edge detection: A neural model for physiological and psychoacoustical responses to amplitude transients. *J. Neurophysiol.* 85: 2303–2323.
- Furukawa S, Xu L, Middlebrooks JC (2000) Coding of sound-source location by ensembles of cortical neurons. *J. Neurosci.* 20: 1216–1228.
- Gaumond RP, Kim DO, Molnar CE (1983) Response of cochlear nerve fibers to brief acoustic stimuli: Role of discharge-history effects. *J. Acoust. Soc. Am.* 74: 1392–1398.
- Gawne TJ, Kjaer TW, Richmond BJ (1996) Latency: Another potential code for feature binding in striate cortex. *J. Neurophysiol.* 76: 1356–1360.
- Geisler CD, Deng L, Greenberg SR (1985) Thresholds for primary auditory fibers using statistically defined criteria. *J. Acoust. Soc. Am.* 77: 1102–1109.
- Glasberg BR, Moore BC (1990) Derivation of auditory filter shapes from notched-noise data. *Hear. Res.* 47: 103–138.
- Haftner ER, Carrier SC (1972) Binaural interaction in low-frequency stimuli: The inability to trade time and intensity completely. *J. Acoust. Soc. Am.* 51: 1852–1862.
- Heffner RS, Heffner HE (1985) Hearing range of the domestic cat. *Hear. Res.* 19: 85–88.
- Heil P (1997a) Auditory cortical onset responses revisited. I. First-spike timing. *J. Neurophysiol.* 77: 2616–2641.
- Heil P (1997b) Auditory cortical onset responses revisited. II. Response strength. *J. Neurophysiol.* 77: 2642–2660.
- Heil P, Irvine DR (1996) On determinants of first-spike latency in auditory cortex. *Neuroreport.* 7: 3073–3076.
- Heil P, Irvine DR (1997) First-spike timing of auditory-nerve fibers and comparison with auditory cortex. *J. Neurophysiol.* 78: 2438–2454.
- Heil P, Irvine DR (1998) The posterior field P of cat auditory cortex: Coding of envelope transients. *Cereb. Cortex.* 8: 125–141.
- Heil P, Neubauer H (2001) Temporal integration of sound pressure determines thresholds of auditory-nerve fibers. *J. Neurosci.* 21: 7404–7415.
- Henry KR, Lewis ER (1992) One-tone suppression in the cochlear nerve of the gerbil. *Hear. Res.* 63: 1–6.
- Hewitt MJ, Meddis R (1991) An evaluation of eight computer models of mammalian inner hair-cell function. *J. Acoust. Soc. Am.* 90: 904–917.
- Ho N, Destexhe A (2000) Synaptic background activity enhances the responsiveness of neocortical pyramidal neurons. *J. Neurophysiol.* 84: 1488–1496.
- Hopfield JJ (1995) Pattern recognition computation using action potential timing for stimulus representation. *Nature* 376: 33–36.
- Horst JW, Javel E, Farley GR (1990) Coding of spectral fine structure in the auditory nerve. II. Level-dependent nonlinear responses. *J. Acoust. Soc. Am.* 88: 2656–2681.

- Johnson DH (1978) The relationship of post-stimulus time and interval histograms to the timing characteristics of spike trains. *Biophys. J.* 22: 413–430.
- Johnson DH (1996) Point process models of single-neuron discharges. *J. Comput. Neurosci.* 3: 275–299.
- Joris PX, Smith PH, Yin TC (1998) Coincidence detection in the auditory system: 50 years after Jeffress. *Neuron* 21: 1235–1238.
- Kitzes LM, Gibson MM, Rose JE, Hind JE (1978) Initial discharge latency and threshold considerations for some neurons in cochlear nuclear complex of the cat. *J. Neurophysiol.* 41: 1165–1182.
- Klug A, Khan A, Burger RM, Bauer EE, Hurley LM, Yang L, Grothe B, Halvorsen MB, Park TJ (2000) Latency as a function of intensity in auditory neurons: Influences of central processing. *Hear. Res.* 148: 107–123.
- Krishna BS, Semple MN (2000) Auditory temporal processing: Responses to sinusoidally amplitude-modulated tones in the inferior colliculus. *J. Neurophysiol.* 84: 255–273.
- Lieberman MC (1978) Auditory-nerve response from cats raised in a low-noise chamber. *J. Acoust. Soc. Am.* 63: 442–455.
- Lieberman MC (1982) Single-neuron labeling in the cat auditory nerve. *Science* 216: 1239–1241.
- Lieberman MC, Dodds LW, Pierce S (1990) Afferent and efferent innervation of the cat cochlea: Quantitative analysis with light and electron microscopy. *J. Comp. Neurol.* 301: 443–460.
- Lowen SB, Teich MC (1992) Auditory-nerve action potentials form a nonrenewal point process over short as well as long time scales. *J. Acoust. Soc. Am.* 92: 803–806.
- Mason AC, Oshinsky ML, Hoy RR (2001) Hyperacute directional hearing in a microscale auditory system. *Nature* 410: 686–690.
- Maunsell JH, Ghose GM, Assad JA, McAdams CJ, Boudreau CE, Noerager BD (1999) Visual response latencies of magnocellular and parvocellular LGN neurons in macaque monkeys. *Vis. Neurosci.* 16: 1–14.
- Merchan-Perez A, Liberman MC (1996) Ultrastructural differences among afferent synapses on cochlear hair cells: Correlations with spontaneous discharge rate. *J. Comp. Neurol.* 371: 208–221.
- Moser T, Beutner D (2000) Kinetics of exocytosis and endocytosis at the cochlear inner hair cell afferent synapse of the mouse. *Proc. Natl. Acad. Sci. USA* 97: 883–888.
- Mountcastle VB, Davies PW, Berman AL (1957) Response properties of neurons of cats somatic sensory cortex to peripheral stimuli. *J. Neurophysiol.* 20: 374–407.
- Neff W, Hind J (1955) Auditory thresholds of the cat. *J. Acoust. Soc. Am.* 27: 480–483.
- Oxenham AJ, Plack CJ (2000) Effects of masker frequency and duration in forward masking: Further evidence for the influence of peripheral nonlinearity. *Hear. Res.* 150: 258–266.
- Panzeri S, Petersen RS, Schultz SR, Lebedev M, Diamond ME (2001) The role of spike timing in the coding of stimulus location in rat somatosensory cortex. *Neuron* 29: 769–777.
- Patterson R, Nimmo-Smith I, Holdsworth J, Rice P (1988) Implementing a gammatone filter bank. SVOS Final Report, The Auditory Filter Bank.
- Phillips DP, Hall SE (1990) Response timing constraints on the cortical representation of sound time structure. *J. Acoust. Soc. Am.* 88: 1403–1411.
- Rajan R, Irvine DR, Cassell JF (1991) Normative N1 audiogram data for the barbiturate-anaesthetised domestic cat. *Hear. Res.* 53: 153–158.
- Reich DS, Mechler F, Victor JD (2001) Temporal coding of contrast in primary visual cortex: When, what, and why. *J. Neurophysiol.* 85: 1039–1050.
- Rhode WS, Recio A (2000) Study of mechanical motions in the basal region of the chinchilla cochlea. *J. Acoust. Soc. Am.* 107: 3317–3332.
- Rhode WS, Smith PH (1985) Characteristics of tone-pip response patterns in relationship to spontaneous rate in cat auditory nerve fibers. *Hear. Res.* 18: 159–168.
- Rieke F, Warland D, de Ruyter van Steveninck R, Bialek B (1997) *Spikes: Exploring the neural code*. MIT Press, Cambridge, MA.
- Rosowski JJ (1991) The effects of external- and middle-ear filtering on auditory threshold and noise-induced hearing loss. *J. Acoust. Soc. Am.* 90: 124–135.
- Sachs MB (1984) Neural coding of complex sounds: Speech. *Annu. Rev. Physiol.* 46: 261–273.
- Sachs MB, Winslow RL, Sokolowski BH (1989) A computational model for rate-level functions from cat auditory-nerve fibers. *Hear. Res.* 41: 61–69.
- Shamma SA, Chadwick RS, Wilbur WJ, Morrish KA, Rinzel J (1986) A biophysical model of cochlear processing: Intensity dependence of pure tone responses. *J. Acoust. Soc. Am.* 80: 133–145.
- Smith RL, Brachman ML (1980) Operating range and maximum response of single auditory nerve fibers. *Brain. Res.* 184: 499–505.
- Snyder DL, Miller MI (1991) *Random Point Processes in Time and Space*. Springer-Verlag, New York.
- Stein RB (1967) Some models of neuronal variability. *Biophys. J.* 7: 37–68.
- Van Rossum MC (2001) The transient precision of integrate and fire neurons: Effect of background activity and noise. *J. Comput. Neurosci.* 10: 303–311.
- Warzecha A, Egelhaaf M (2000) Response latency of a motion-sensitive neuron in the fly visual system: Dependence on stimulus parameters and physiological conditions. *Vision Res.* 40: 2973–2983.
- Weiss TF, Rose C (1988) A comparison of synchronization filters in different auditory receptor organs. *Hear. Res.* 33: 175–179.
- Yates GK (1991) Auditory-nerve spontaneous rates vary predictably with threshold. *Hear. Res.* 57: 57–62.